Linear stability analysis of convective chemical fronts

Desiderio A. Vasquez
Department of Physics, Indiana University–Purdue University Fort Wayne, Fort Wayne, Indiana 46805-1499
(Received 23 April 1997; revised manuscript received 25 July 1997)

A chemical front propagating upward in a fluid separates heavy unreacted fluid from light reacted fluid. The density difference caused by the front propagation leads to convection. Convection enhances the front speed and curves the front as it propagates upward in a tube. The convective front propagates with constant speed and is steady in a frame of reference comoving with the front. This paper presents a linear stability analysis of the convective front. The fronts are modeled using a front evolution equation coupled to Darcy's law for flow in porous media and the Navier-Stokes for viscous flow. The solutions can be either axisymmetric or nonaxisymmetric as observed in experiments in tubes. For flow in porous media, there is a region of bistability between both types, whereas in viscous flow the axisymmetric front is always unstable. [S1063-651X(97)07412-6]

PACS number(s): 47.20.Bp, 47.54.+r, 47.70.Fw, 03.40.Gc

I. INTRODUCTION

Chemical waves generate thermal and compositional gradients that lead to convection. Recent experimental and theoretical work have shown that convection significantly alters the behavior of the chemical wave. Miike, Muller, and Hess showed that convective rolls are associated with the chemical waves in the Belousov-Zhabotinsky (BZ) reaction [1]. Menzinger *et al.* observed convective turbulence as the BZ reaction takes place in a vertical tube [2]. Chemical waves propagating upward are different than propagating downward due to convection in the iron (II)-nitric acid reaction [3], the chlorite-thiosulfate reaction [4], and the iodate-arsenous acid reaction in vertical cylinders [5]. Experiments by Masere *et al.* in the iodate-arsenous acid reaction showed that a front propagating upward in a vertical cylinder can be either flat, nonaxisymmetric, or axisymmetric depending on the diameter of the tube [6]. For diameters less than 1.1 mm, the front is flat; if the diameter is between 1.1 and 2.3 mm, the front is nonaxisymmetric; and for larger diameters the front is axisymmetric. Fronts propagating downward are always flat with the same speed. They have the same speed of the flat front propagating upward, indicating no convection, thus the curvature of the front and speed enhancement is due to convective fluid motion. In this reaction, a single front propagating upward separates heavy unreacted fluid from light reacted fluid. This density difference leads to convection.

Previous theoretical work consisted of the linear stability analysis of the convectionless flat fronts in the iodate-arsenous reaction [7]. This calculation showed that the flat front is unstable to nonaxisymmetric perturbations near the onset of convection, and unstable to axisymmetric perturbations for larger diameters [8]. However, this calculation cannot predict when the transition from a nonaxisymmetric to an axisymmetric front takes place. In order to describe this process, a linear stability analysis of the convective fronts is required. Theoretical work on convective fronts in the iodate-arsenous acid reaction consisted of numerical solutions of the equations of motion in two dimensions. The front was modeled with reaction-diffusion equations [9] and with a front evolution equation [10]. The reaction-diffusion solutions are computationally more expensive, but they showed the transition from flat, to nonaxisymmetric, and later to axisymmetric fronts as the width of the tube is increased [11]. The solutions of the front evolution equations showed only nonaxisymmetric fronts.

Theoretical work for flow in porous media are relevant to experiments where the reaction takes place between two vertical walls, a Hele-Shaw cell [12]. The reaction-diffusion equation coupled to Darcy's law showed a region of bistability where the front can be either axisymmetric or nonaxisymmetric [13]. This property was not observed for the viscous fluid equations described by the Navier-Stokes equations. In this work, we carry out the linear stability analysis of convective fronts using the front evolution equation. We considered flow in porous media using Darcy's law, and viscous flow using the Navier-Stokes equations.

II. EQUATIONS OF MOTION

Chemical waves in the iodate-arsenous reaction are described with a reaction-diffusion equation coupled to nonlinear hydrodynamics. Numerical solutions on a two-dimensional grid showed transitions from flat, to nonaxisymmetric, and later to axisymmetric fronts [11]. In the present work, the chemical front is described with an eikonal relation that gives the normal velocity of the reaction front (c) as a function of the local curvature (K):

$$c = c_0 + D_c K + \vec{V} \cdot \hat{n}. \tag{1}$$

Here c_0 is the flat front speed, D_c is the molecular diffusivity, $\vec{V}$ is the fluid velocity, and $\hat{n}$ is the normal unit vector to the front. The eikonal relation was first introduced by Zykov [14], and later used by Keener and Tyson in the context of the Belousov-Zhabotinsky reaction [15]. The relation was mathematically derived from a set of reaction-diffusion equations using singular perturbation theory [16]. This relation was verified in experiments by Foerster, Muller, and Hess [17]. Wilder, Vasquez, and Edwards showed that this model can be applied to chemical waves involving fluid flow [18].

The front can be described by the front height $z=H(x,t)$, where x is the horizontal coordinate, and z the vertical coordinate. We consider only the two-dimensional problem in the x-z plane. The curvature can be expressed as a function of H,

$$K=\frac{\partial^2 H/\partial x^2}{[1+(\partial H/\partial x)^2]^{1/2}}, \tag{2}$$

as well as the normal unit vector:

$$\hat{n}=\frac{[\hat{z}-(\partial H/\partial x)\hat{x}]}{[1+(\partial H/\partial x)^2]^{1/2}}. \tag{3}$$

Here $\hat{x}$ and $\hat{z}$ are the unit vectors in the x and z directions, respectively.

For fluid in porous media or viscous fluid between two vertical slabs with a narrow gap, the flow can be described with Darcy's law

$$\vec{V}=-\frac{k}{\mu}(\vec{\nabla}P+\rho g\hat{z}), \tag{4}$$

and the continuity equation

$$\nabla\cdot\vec{V}=0. \tag{5}$$

Here $\vec{V}$ is the fluid velocity, P is the pressure, g is the acceleration of gravity in the vertical z direction, k is the coefficient of permeability of the medium, and μ is the coefficient of viscosity. For viscous fluid in a Hele-Shaw cell, we just have to replace k with $a^2/12$, where a is the slab width. The fluid density (ρ) is included only where it modifies the large gravity term. Using a step function Θ, which is zero if the argument is negative and 1 if it is positive, we can write the fluid density as

$$\rho=\rho_0+\Delta\rho\Theta(z-H). \tag{6}$$

The continuity equation allows us to replace the fluid velocity with a stream function, where the components of the velocity are given by

$$V_x=\frac{\partial\psi}{\partial z} \quad \text{and} \quad V_z=-\frac{\partial\psi}{\partial x}. \tag{7}$$

With this substitution, Darcy's law becomes

$$\nabla^2\psi=-\frac{k}{\mu}g\frac{\partial\rho}{\partial x}. \tag{8}$$

The derivative of the step function in the density ρ leads to a Dirac δ function, which in turn determines jump conditions for the stream function across the front. The equation for the stream function is then the Laplace equation

$$\nabla^2\psi=0, \tag{9}$$

with jump conditions across the front:

$$[\psi]_H=0, \tag{10}$$

$$\left[\frac{d\psi}{dz}\right]_H=\tilde{R}\frac{\partial H}{\partial x}, \tag{11}$$

with

$$\tilde{R}=\frac{k}{\mu}g\Delta\rho. \tag{12}$$

The brackets indicate the value of any function in the unreacted side of the front, minus the value in the reacted side of the front.

The equations of motion and the boundary conditions can be further simplified using a reference frame moving with the speed of the flat front, and considering only small deviations from the flat front. In this reference frame Eqs. (9)–(11) still govern the behavior of the stream function; however, the stream function relates to the increase of speed of the fluid flow. The fluid velocity in the moving frame is $\vec{V}_0=-c_0\hat{z}$, so Eq. (7) just gives the additional velocity to this field. Thus the solution for a flat convectionless front is given by $H=0$ and $\vec{V}=0$, since the total fluid velocity is equal to $\vec{V}_0+\vec{V}$. Equations (9)–(11) indicate that the stream function depends linearly with $\partial H/\partial x$. Using this fact, and expanding the normal vector $\hat{n}$ and the curvature K up to second order in $\partial H/\partial x$, we obtain a front propagation equation

$$\frac{\partial H}{\partial t}=D\frac{\partial^2 H}{\partial x^2}+\frac{c_0}{2}\left(\frac{\partial H}{\partial x}\right)^2+V_z|_{z=H}. \tag{13}$$

We can relate the jump conditions at the front to jump conditions at $z=0$ using a Taylor expansion of the form

$$[\xi]_{z=H}=[\xi]_{z=0}+H\left[\frac{\partial\xi}{\partial z}\right]_{z=0}+\cdots. \tag{14}$$

Here ξ represents any variable that needs to be matched at the front. The front height H is considered small. In the jump conditions [Eqs. (10) and (11)], the fluid variables ψ and $\partial\psi/\partial z$ are already proportional to H, therefore, the second term in the Taylor expansion [Eq. (12)] will be of order $o(H^2)$. Since we just need to include linear terms on H in the fluid velocity V_z [Eq. (11)], we can approximate

$$[\xi]_{z=H}=[\xi]_{z=0}. \tag{15}$$

Using similar arguments based on a Taylor expansion, we can use $V|_{z=0}$, in Eq. (13) instead of $V|_{z=H}$. Therefore the jump conditions can be taken at $z=0$, as well as the vertical component of the fluid velocity.

The front evolution equations in a viscous fluid was derived in a previous work [19]. The only difference is replacing Darcy's law (Eq. 4) with the linearized Navier-Stokes equations in a frame comoving with the flat front. In terms of the stream function,

$$c_0\frac{\partial}{\partial z}\nabla^2\psi+\nu\nabla^2\nabla^2\psi=0, \tag{16}$$

together with the jump conditions

$$[\psi]_0 = 0, \tag{17}$$

$$\left[\frac{\partial \psi}{\partial z}\right]_0 = 0, \tag{18}$$

$$\left[\frac{\partial^2 \psi}{\partial z^2}\right]_0 = 0, \tag{19}$$

$$\left[\frac{\partial^3 \psi}{\partial z^3}\right]_0 = \frac{g\Delta\rho}{\nu\rho_0}\frac{\partial H}{\partial x}. \tag{20}$$

Here ν is the kinematic viscosity, and is related to the coefficient of viscosity by $\nu = \mu/\rho$. The boundary conditions for Darcy's law requires that the normal fluid velocity at the walls vanish. For viscous fluids, we choose free slip boundaries, which also require vanishing normal velocity at the walls. This will allow us to compare both models under the same boundary conditions.

III. SOLUTIONS FOR FLOW IN POROUS MEDIA

We solve the equations of motion for flow in porous media introducing a Fourier expansion on the stream function (ψ) and the front height (H):

$$\psi(x,z,t) = \sum_n \psi_n(z,t)\sin(nqx), \tag{21}$$

$$H(x,t) = \sum_n H_n(t)\cos(nqx). \tag{22}$$

The boundaries are two vertical walls located at $x=0$ and $x=L$. The number q is determined by the wall separation $q=\pi/L$. With these substitutions Eqs. (9)–(11) are decoupled into equations for the Fourier coefficients:

$$\frac{d^2\psi_n}{dz^2} - (nq)^2\psi_n = 0, \tag{23}$$

$$[\psi_n]_0 = 0, \tag{24}$$

$$\left[\frac{d\psi_n}{dz}\right]_0 = -\widetilde{R}(nq)H_n. \tag{25}$$

This set of equations with the jump conditions can be solved as functions of H_n:

$$\psi_n(z) = \begin{cases} \dfrac{\widetilde{R}H_n}{2}e^{(nqz)} & \text{if } z<0 \\ \dfrac{\widetilde{R}H_n}{2}e^{-(nqz)} & \text{if } z\geq 0. \end{cases} \tag{26}$$

Using this result together with the relation between the vertical component of the velocity and the stream function, we can write the front evolution equation using only the front height H and its Fourier coefficients:

$$\frac{\partial H}{\partial t} = D\frac{\partial^2 H}{\partial x^2} + \frac{c_0}{2}\left(\frac{\partial H}{\partial x}\right)^2 + \frac{\widetilde{R}}{2}\sum_n (nq)H_n\cos(nqx). \tag{27}$$

We define dimensionless units:

$$H = (D/c_0)H', \tag{28}$$

$$x = x'D/\widetilde{R}, \tag{29}$$

$$q = q'\widetilde{R}/D, \tag{30}$$

$$t = t'D/\widetilde{R}^2, \tag{31}$$

$$v' = c_0^2/\widetilde{R}^2 \tag{32}$$

to transform the equation into

$$\frac{\partial H'}{\partial t'} = \frac{\partial^2 H'}{\partial x'^2} + \frac{1}{2}\left(\frac{\partial H'}{\partial x'}\right)^2 + \sum_n \frac{(nq')}{2}H_n'\cos(nq'x'). \tag{33}$$

From now on we will drop the primes. The reason for this choice of units is clear, as we introduce the Fourier expansion [Eq. (22)] to transform the partial differential equations into a set of ordinary differential equations (ODE's) on the Fourier coefficients H_n. The resulting set of ODE's does not contain the term v_0 except on the projection over H_0:

$$\frac{dH_0}{dt} = \frac{q^2}{4}\sum_{n=1} n^2H_n^2, \tag{34}$$

$$\frac{dH_p}{dt} = \left(-p^2q^2 + \frac{pq}{2}\right)H_p + \frac{q^2}{4}\sum_{n=1}\sum_{m=1} nmH_nH_m \times(\delta_{p,|n-m|} - \delta_{p,n+m}) \quad \text{for } p\geq 1. \tag{35}$$

This means that the behavior of the dynamical system is determined solely by the coefficients H_n with $n>0$, with their behavior independent from the dimensionless flat front speed. They will be determined only by the dimensionless parameter q which is related to the width of the tube. We can obtain valuable insight in the stability of the fronts just by keeping a few terms in the truncations. A two term truncation

$$\frac{dH_0}{dt} = q^2H_1^2/4, \tag{36}$$

$$\frac{dH_1}{dt} = -q^2H_1 + \frac{1}{2}qH_1 \tag{37}$$

is useful to analyze the stability of the flat front. The first equation determines the behavior of H_0. The second equation is a linear equation involving only H_1. To analyze the stability of the flat front solution ($H_0=0$ and $H_1=0$) it is necessary to analyze the stability of the second equation involving only H_1. The solution is stable only if $q>\frac{1}{2}$, which is the result of a previous linear stablity analysis [20]. For

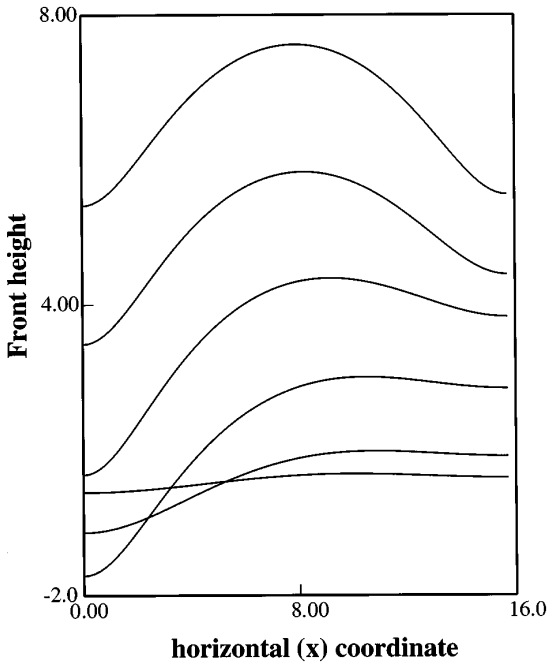

FIG. 1. Time sequence showing the development of the convective front from a perturbed flat front in porous media. We show the front every 30 dimensionless time units. In this case, an axisymmetric front develops. The spatial units are the dimensionless spatial units defined in the text. The reference frame is moving with the flat front speed.

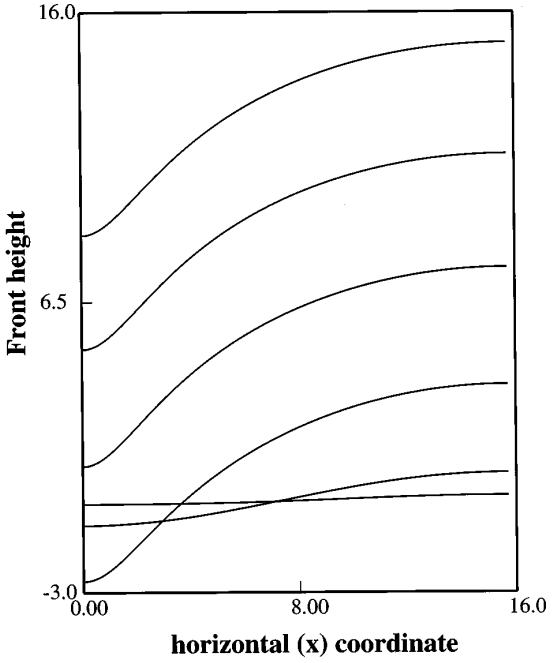

FIG. 2. Time sequence showing the development of the convective front from a perturbed flat front in porous media. We show the front every 30 dimensionless time units. In this case, a nonaxisymmetric front develops. The spatial units are the dimensionless spatial units defined in the text. The reference frame is moving with the flat front speed.

unstable solutions, the coefficient H_1 grows exponentially, forcing H_0 to grow because of their coupling through the first equation. In this case there is no stable curved front. A three term truncation

$$\frac{dH_0}{dt} = q^2 H_1^2/4 + q^2 H_2^2, \tag{38}$$

$$\frac{dH_1}{dt} = -q^2 H_1 + q^2 H_1 H_2 + \tfrac{1}{2} q H_1, \tag{39}$$

$$\frac{dH_2}{dt} = -4q^2 H_2 - \tfrac{1}{4} q^2 H_1^2 + q H_2 \tag{40}$$

provides the nonlinear mechanism that stabilizes the convective front. In this system, the behavior of H_0 is determined by the coefficients H_1 and H_2. The other equations do not involve H_0. The flat front solution ($H_0 = v_0 t$ with $H_1 = H_2 = 0$) is also stable for $q > \frac{1}{2}$ which is determined by the second and third equations. A steady state solution for the last two equations can be found with $H_2 = (2q-1)/2q$ and $H_1^2 = 2(-2q+1)(4q-1)/q^2$, these formulas require that $q < \frac{1}{2}$ for the solution to exist. Linearizing the equations shows that the solution is stable for $q > \frac{1}{4}$. In summary, the three-term truncation shows a transition from a stable flat front ($q > \frac{1}{2}$), to a stable convective front ($\frac{1}{4} < q < \frac{1}{2}$), to an unstable convective front ($q < \frac{1}{4}$).

With 25 terms in the truncation we obtain axisymmetric fronts as well as nonaxisymmetric fronts. A direct numerical simulation with $q = 0.2$ generates both types of fronts starting with small random perturbations. The flat front evolves into either front depending on the initial conditions. In Fig. 1, we show the evolution of a flat front with small random perturbations leading to an axisymmetric front. The height of the front is measured in a reference frame comoving with the speed of the convectionless flat front (v_0). In other words, a horizontal line at $H = 0$ represents the moving flat front. The curved front moves with a speed faster than the flat front speed, increasing steadily its average height. In Fig. 2 we show the results obtained with different random initial perturbations. In this case a nonaxisymmetric front evolves from the initial front. We observe that the speed of the nonaxisymmetric front is higher by comparing the positions of the axisymmetric front with the nonaxisymmetric front at exactly the same times after initiation. Both fronts are stable for the same parameter q, which indicates that bistability exists.

Convection causes the different shapes of the front. For a nonaxisymmetric front, one convective roll is present as shown in Fig. 3. In this case, fluid rises close to one vertical wall, falling close to the opposite wall, causing the characteristic nonaxisymmetric shape. In the case of an axisymmetric front (Fig. 4), we find that the fluid rises in the middle and falls near the walls. The front is completely symmetric for a reflection around a vertical line through the middle of the tube. This is shown in the steady state solution of Eqs. (35) where only the Fourier coefficients for even symmetry are present, namely, the coefficients H_n, with n even. For the nonaxisymmetric front, both even and odd terms are present. Consequently, the front is not antisymmetric.

We carry out the linear stability analysis of the convective front to understand the bistability observed in the numerical solutions. First, we obtain the numerical solution of each

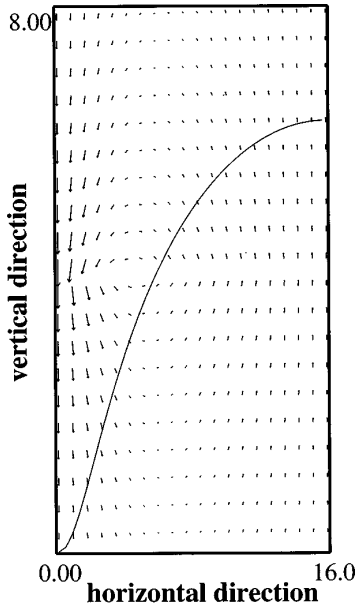

FIG. 3. Velocity field near a nonaxisymmetric front in porous media. The front curvature is caused by fluid rising near one wall and falling near the opposing wall. The units are the dimensionless units described in the text. The reference frame is moving with the flat front speed.

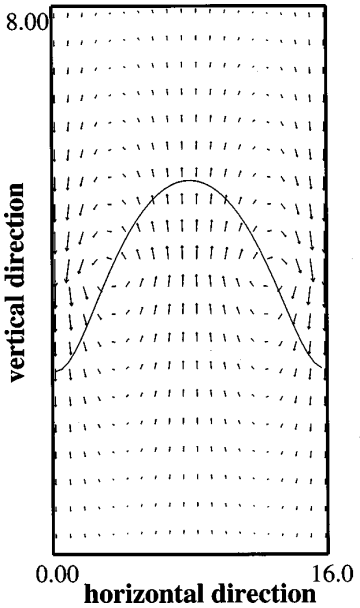

FIG. 4. Velocity field near an axisymmetric front in porous media. The front curvature is caused by fluid rising in the middle and falling near the walls. The units are the dimensionless units described in the text. The reference frame is moving with the flat front speed.

front using Newton's method for the system of nonlinear equations [21]. These steady state solutions correspond to setting the time derivatives to zero in Eqs. (35). We use an axisymmetric solution to start Newton's method, with the value of q slightly changed. In this way we obtain a branch of axisymmetric solutions as q varies (Fig. 5). We tested the result comparing the solution of Newton's method with the solution of the direct numerical simulation of the ODE's. The results are the same. We proceed in the same manner to generate the nonaxisymmetric branch. The calculated axisymmetric branch runs from $q=0.12$ to 0.23. No solution was found for values above $q=0.23$. While solutions for values with $q<0.1$ are possible in both branches, we chose not to study them beyond this point. Small values of q lead to fronts with very high curvature. The front evolution model is an approximation of the eikonal relation for a small curvature. In this regime, the full eikonal relation may be needed, as well as the inclusion of more terms in the truncation for accurate solutions. The nonaxisymmetric branch was calculated from $q=0.5$ (where the transition from flat to convective front takes place) to $q=0.12$. The speeds of both types of fronts always increase as q decreases. This means that as the tube is widened the front moves faster. However, the speed of the axisymmetric front can be lower than the speed of the nonaxisymmetric front for a small range of values of q in the regime where both types are stable.

The linear stability analysis is carried out linearizing the equations around these solutions. We use the routines in the EISPACK diagonalization package to calculate the corresponding eigenvalues [22]. The real part of the eigenvalues determines the stability of the front, consequently we need to study only the eigenvalue with a maximum real part. If the maximum real part of the eigenvalue is positive the front is unstable, if it is negative it implies that all the real parts are negative, thus the front is stable. The results are summarized in Fig. 6 where we plot the real part of the eigenvalue with a maximum real part, as a function of the parameter q. For $0.17<q<0.5$ the nonaxisymmetric solution is stable as the real part of the eigenvalue is positive. For $0.23<q<0.25$ there is an unstable axisymmetric solution, while for $q<0.25$ we found a stable axisymmetric solution.

IV. SOLUTIONS FOR VISCOUS FLOW

The equations of motion coupled to the jump conditions for viscous flow lead to the front evolution equation coupled

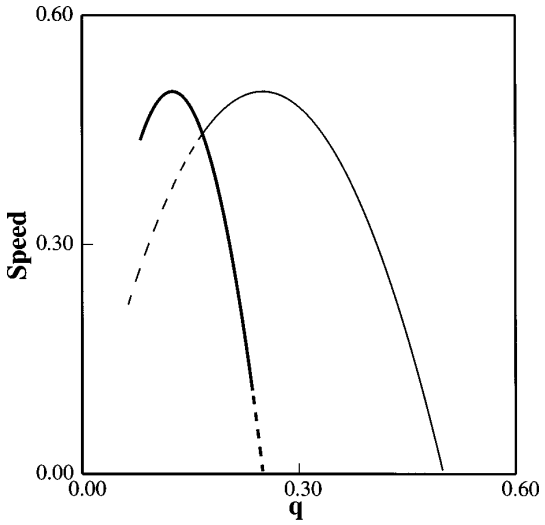

FIG. 5. The front speed as a function of the number $q=\pi/L$ in a porous media. The solid line corresponds to stable fronts, and the dotted line to unstable fronts. The bold line is for axisymmetric fronts, and the thin line is for nonaxisymmetric fronts. There is a change of stabilities in each branch. The speed is measured relative to the flat front speed. The units are the dimensionless units described in the text.

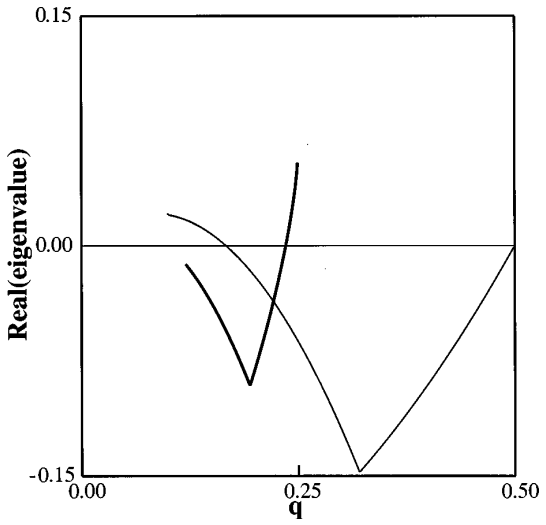

FIG. 6. Maximum real part for the eigenvalues of the linearized matrix around the convective front solutions in porous media. The thin line corresponds to the nonaxisymmetric solution. It is negative for $0.17<q<0.5$, indicating a stable front. The bold line corresponds to the axisymmetric solution. It is negative for $q<0.23$.

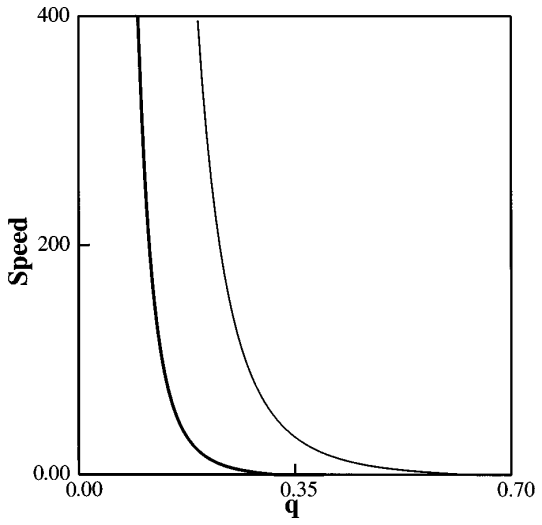

FIG. 7. The front speed as a function of the number $q=\pi/L$ in a viscous fluid. The thin line corresponds to an unstable axisymmetric front, while the bold line corresponds to a stable nonaxisymmetric front. The speed is measured relative to the flat front speed. The units are the dimensionless units described in the text.

to the front Fourier coefficients H_n:

$$\frac{\partial H}{\partial t}=D\frac{\partial^2 H}{\partial x^2}+\frac{c_0}{2}\left(\frac{\partial H}{\partial x}\right)^2+\frac{R_f}{4}\sum_n \frac{H_n}{nq}\cos(nqx), \tag{41}$$

with

$$R_f=\frac{g\Delta\rho}{\nu\rho_0}. \tag{42}$$

The derivation of this equation is similar to the derivation of Eqs. (33), and can be found in the literature [19]. This equation is an approximation valid for the experimental parameters of the iodate-arsenous acid reaction, where the speed of the front can be neglected for values of q near the onset of convection [7]. We introduce the dimensionless units for viscous fluid:

$$H=(D/c_0)H', \tag{43}$$

$$x=x'\left(\frac{D}{R_f}\right)^{1/3}, \tag{44}$$

$$q=q'\left(\frac{R_f}{D}\right)^{1/3}, \tag{45}$$

$$t=t'\frac{c_0}{D^{2/3}R_f^{1/3}}, \tag{46}$$

$$v_0'=\frac{c_0^2}{D^{4/3}R_f^{2/3}}. \tag{47}$$

With these units, the resulting set of ODE's on the Fourier coefficients is

$$\frac{dH_p}{dt}=\left(-p^2q^2+\frac{1}{4pq}\right)H_p+\frac{q^2}{4}\sum_{n=1}\sum_{m=1} nmH_nH_m \times(\delta_{p,|n-m|}-\delta_{p,n+m}) \quad \text{for } p\geq 1, \tag{48}$$

with the equation for H_0 identical to its corresponding equation for a porous media [Eq. (31)].

We look for the steady state solutions using the techniques previously described. The results are shown in Fig. 7, where we display the speed of the axisymmetric and nonaxisymmetric branches as functions of the parameter q. The calculations used a 125-term truncation required to assure convergence. We find two types of steady state solutions. The nonaxisymmetric solutions are possible with $q<0.63$, the axisymmetric solutions are possible with $q<0.32$. The nonaxisymmetric state includes terms of even and odd parity in the Fourier expansion, while the axisymmetric state contains only even terms, as was the case for flow in porous media. The calculation of the eigenvalues (Fig. 8) show that the nonaxisymmetric steady state is always stable, while the axisymmetric state is always unstable. There is no region of bistability as it was the case of flow in porous media.

V. DISCUSSION AND CONCLUSIONS

Newton's method provided the convective steady state solutions of the front evolution equations. A linear stability analysis determined the stability of these solutions. The calculation of the maximum real part of the eigenvalues indicated a transition from flat fronts to nonaxisymmetric fronts, as well as the parameters where the axisymmetric fronts become stable for fronts propagating in porous media or Hele-Shaw cells. Moreover, a region of bistability between axisymmetric fronts and nonaxisymmetric fronts was observed. This bistability was also observed in fronts modeled with a one-variable reaction-diffusion equation coupled to Darcy's law. Carey, Morris, and Kolodner carried out experiments in Hele-Shaw cells, where Darcy's law can be applied [12]. However, a direct comparison with our theory is not yet

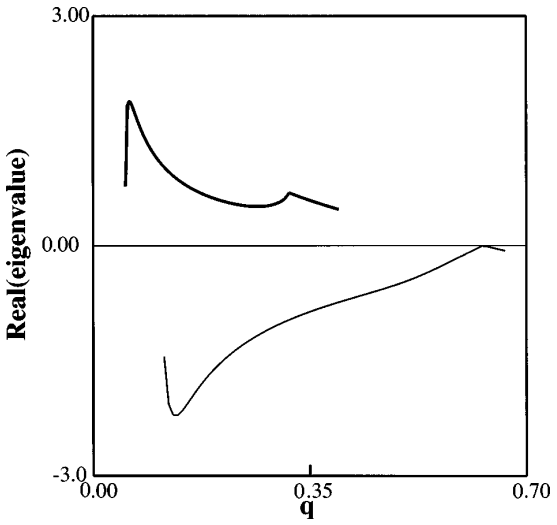

FIG. 8. Maximum real part for the eigenvalues of the linearized matrix around the convective front solutions in a viscous fluid. The thin line corresponds to the nonaxisymmetric solutions. The bold line corresponds to the axisymmetric solutions. The axisymmetric solutions always have a positive real part, consequently they are unstable.

possible, since the experiments were carried out away from the onset of convection. Using the linear stability analysis and the experimental values of the parameters, the onset of convection for a wall separation of 0.05 cm has a critical slab width of 0.06 cm. The bistable region should lie close to twice that length (0.12 cm). The actual experiments have slab widths of 3.2 cm. This means that the experiments in Hele-Shaw cells were performed not only above onset, but also well above the region of bistability. New experiments will have to be designed to test the onset of convection and the predicted bistability. However, since the critical wave number (q_c) for the onset of convection varies by a factor of about 2 between the front evolution model and the reaction-diffusion model [13], the front evolution model may only have a qualitative comparison with the experiments. We point out that both models have the same qualitative features, namely, a nonaxisymmetric front near the onset of convection, and a region of bistability away from onset.

The linear stability analysis of the convective fronts in viscous fluids establish that there are stable nonaxisymmetric fronts near the onset of convection. However, it also establishes that there are no stable axisymmetric fronts. This is contrary to what is observed in the experiments, where nonaxisymmetric fronts are observed near the onset of convection, and axisymmetric fronts are observed away from the onset of convection. This result helps to explain a previous numerical simulation of the front evolution equation using the correct no-flow boundary conditions in a two-dimensional slab [10]. This study found that the calculated front speed was comparable to the experimental front speed near the onset of convection. However, it did not find axisymmetric fronts. Axisymmetric fronts appeared in direct numerical simulations using the reaction-diffusion equation to describe the iodate-arsenous acid reaction front [11]. This indicates that the front evolution model is not reliable beyond the onset of convection. Nevertheless, both models roughly agree for the critical wavelength for the onset of convection. The qualitative and quantitative features of the front evolution equation with viscous fluids are valid only near the onset of convection.

ACKNOWLEDGMENTS

This research was supported by a grant from Research Corporation. Helpful discussions with Joseph Wilder are also acknowledged. I acknowledge the Pontificia Universidad Catolica del Peru for their generous allotment of time during the writing of the manuscript.

[1] H. Miike, S. C. Muller, and B. Hess, Phys. Lett. A **141**, 25 (1989).
[2] M. Menzinger, A. Tzalmona, R. L. Armstrong, A. Cross, and C. Lemaire, J. Phys. Chem. **96**, 4725 (1992).
[3] I. Nagypal, G. Bazsa, and I. R. Epstein, J. Am. Chem. Soc. **108**, 3635 (1986).
[4] G. Bazsa and I. R. Epstein, J. Phys. Chem. **89**, 3050 (1985); J. A. Pojman and I. R. Epstein, *ibid.* **95**, 1306 (1991).
[5] T. McManus, Ph.D. thesis, West Virginia University, 1989; J. A. Pojman, I. R. Epstein, T. J. McManus, and K. Showalter, J. Phys. Chem. **95**, 1299 (1991).
[6] J. Masere, D. A. Vasquez, B. F. Edwards, J. W. Wilder, and K. Showater, J. Phys. Chem. **98**, 6505 (1994)
[7] B. F. Edwards, J. W. Wilder, and K. Showalter, Phys. Rev. A **43**, 749 (1991).
[8] D. A. Vasquez, J. W. Wilder, and B. F. Edwards, Phys. Fluids A **4**, 2410 (1992).
[9] D. A. Vasquez, J. M. Littley, J. W. Wilder, and B. F. Edwards, Phys. Rev. E **50**, 280 (1994).
[10] J. W. Wilder, D. A. Vasquez, and B. F. Edwards, Physica D **90**, 170 (1996).
[11] Y. Wu, D. A. Vasquez, J. W. Wilder, and B. F. Edwards, Phys. Rev. E **52**, 6175 (1995).
[12] M. R. Carey, S. W. Morris, and P. Kolodner, Phys. Rev. E **53**, 6012 (1996).
[13] D. A. Vasquez, J. W. Wilder, and B. F. Edwards, J. Phys. Chem. **104**, 926 (1996).
[14] B. S. Zykov, Biophysics **25**, 329 (1980).
[15] J. P. Keener and J. J. Tyson, Physica D **21**, 307 (1986).
[16] J. J. Tyson and J. P. Keener, Physica D **32**, 327 (1988).
[17] P. Foerster, S. C. Muller, and B. Hess, Science **241**, 685 (1988).
[18] J. W. Wilder, D. A. Vasquez, and B. F. Edwards, Phys. Rev. E **47**, 3761 (1993).
[19] J. W. Wilder, D. A. Vasquez, B. F. Edwards, and G. I. Sivashinsky, Physica D **73**, 217 (1994).
[20] J. Huang, D. A. Vasquez, B. F. Edwards, and P. Kolodner, Phys. Rev. E **48**, 4378 (1993).
[21] W. H. Press, S. A. Teukolsky, W. T. Vetterling, and B. P. Flannery, *Numerical Recipes in Fortran*, 2nd ed. (Cambridge University Press, Cambridge, 1992).
[22] B. T. Smith, J. M. Boyle, J. J. Dongarra, B. S. Garbow, Y. Ikebe, V. C. Klema, and C. B. Moler, *Matrix Eigensystem Routines—EISPACK Guide*, 2nd ed. (Springer-Verlag, Berlin, 1976).